ACS APPLIED MATERIALS & INTERFACES

RESEARCH ARTICLE

www.acsami.org

Preparation of Single-Walled Carbon Nanotube/Silicon Composites and Their Lithium Storage Properties

Ji-Yong Eom† and Hyuk-Sang Kwon*

Department of Materials Science & Engineering, KAIST, 373-1 Guseong-dong, Yuseong-gu, Daejeon 305-701, Korea

ABSTRACT: Single-walled carbon nanotube (SWCNT)/silicon composites were produced from the purified SWCNTs and Si powder by high-energy ball-milling and then electrochemically inserted with Li using Li/(SWCNT/Si) cells. The highest reversible capacity and lowest irreversible capacity of the SWCNT/Si composites were measured to be 1845 and 474 mAh g^{-1} after ball-milling for 60 min, respectively. During the charge/discharge process, most of the Li ions were inserted into the SWCNT/Si composites by alloying with Si particles below 0.2 V and extracted from the SWCNT/Si composites by dealloying with Si particles around 0.5 V. The enhanced capacity and cycle performance of the SWCNT/Si composites produced by high-energy ball-milling were due primarily to the fact that SWCNTs provided a flexible conductive matrix, which compensated for the dimensional changes of Si particles during Li insertion and avoided loosening of the interparticle contacts during the crumbling of Si particles. The ball-milling contributed to a decrease in the particle size of SWCNTs and Si particles and to an increase in the electrical contact between SWCNTs and Si particles in the SWCNT/Si composites.

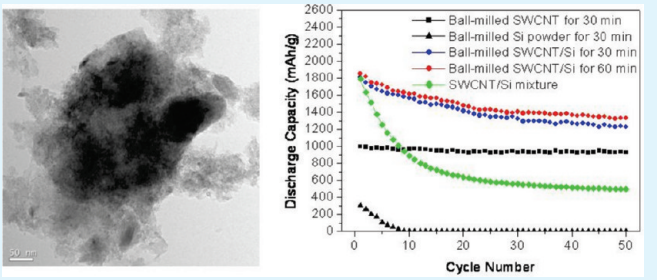

KEYWORDS: single-walled carbon nanotube, silicon, ball-milling, anode, Li-ion battery

1. INTRODUCTION

Carbon nanotubes (CNTs), multiwalled carbon nanotubes (MWCNTs), and single-walled carbon nanotubes (SWCNTs), with a one-dimensional (1D) host lattice structure, have received much attention as a Li-insertion host material in high-energy-density Li-ion rechargeable batteries. The MWCNTs prepared by various synthesis conditions,[1−3] thermal oxidation treatments,[4−6] chemical etching,[7] and mechanical ball-milling[8] have exhibited Li reversible capacities of 80−680 mAh g^{-1} ($Li_{0.2}C_6 \sim Li_{1.8}C_6$). The Li reversible capacities of the raw and purified SWCNTs are reported to be 450−600 mAh g^{-1} ($Li_{1.2}C_6 \sim Li_{1.6}C_6$)[9,10] and increase to 790−1000 mAh g^{-1} ($Li_{2.1}C_6 \sim Li_{2.7}C_6$) by either mechanical ball-milling[11,12] or chemical etching.[13,14] Although the Li reversible capacity of CNTs is higher than that of graphite, 372 mAh g^{-1} (LiC_6), the irreversible capacity is still very high. Also, a large voltage hysteresis appears during the charge/discharge process. These factors, the large irreversible capacity and voltage hysteresis, result in a limited application of CNTs for anode materials in Li-ion batteries.

It is also well-known that Si is alloyed with Li up to 4.4 Li atoms per Si atom at a relatively high temperature, which is equal to the Li storage capacity of 4000 mAh g^{-1}.[15,16] However, the reversibility of normal Si powder at room temperature is poor, because Si is easily crumbled due to large volume expansion during Li insertion and brittleness of the intermetallic Li phase,[15,17] which loses electrical contact. It is reported that the crumbling rate of Si may be delayed when the Si host particles are nanosized[15,16,18,19] or when the buffering components are added.[20] Among the buffering materials, carbonaceous materials such as graphite and CNTs are very promising candidates because of their buffering effects and high conductivity.

It is reported that the Si/graphite composites produced by ball-milling have a large reversible capacity of 1039 mAh g^{-1}, but the cycle performance is still poor.[20] Also, the Si/MWCNT[21,22] and Si/carbon or graphite or VGCF/MWCNT composites[23−25] prepared by various synthesis methods are considered as an anode for high-energy-density Li-ion rechargeable batteries. The MWCNTs of 10−35 wt % added in the composites suppress the crumbling of Si and enhance the cycle performance of the composites. The Si/MWCNT composites in which the MWCNTs are grown on the surface of Si particles have large reversible capacities of 1100−1500 mAh g^{-1} and maintain 80% of their initial reversible capacity after 20 cycles.[21,22] As other approaches, the Si/carbon or graphite or VGCF/MWCNT composites also have large reversible capacities of 1200−1500 mAh g^{-1} and maintain 33−83% of their initial reversible capacity after 20 cycles.[23−25]

The ball-milled CNTs have larger Li storage capacities and higher electron conductivities than the ball-milled graphite.[8,11,12] In addition, it is expected that CNTs maintain contact with Si particles effectively because of their wirelike shape when CNTs and Si particles are compounded. Therefore, it is believed that the benefits of the CNT/Si composites (the high volumetric energy density and Li storage capacity of Si and the good conductivity

Received: November 1, 2010
Accepted: March 8, 2011
Published: March 24, 2011

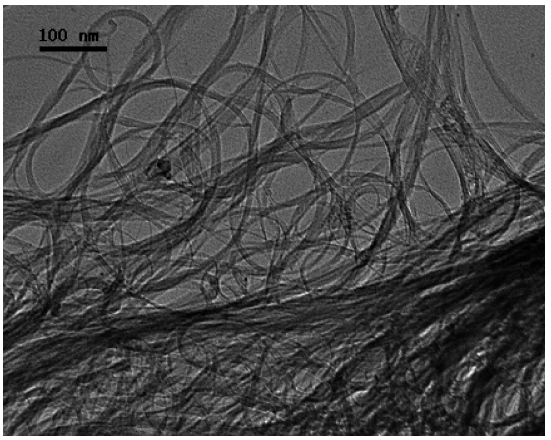

Figure 1. TEM image of the purified SWCNTs.

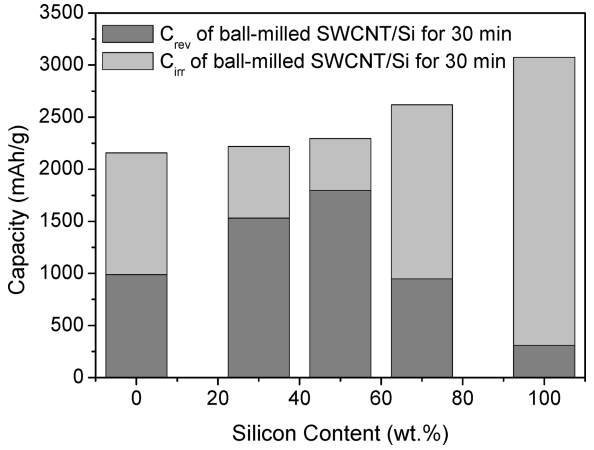

Figure 2. Change in the reversible capacity (C_{rev}) and the irreversible capacity (C_{irr}) of the SWCNT/Si composites after ball-milling for 30 min as a function of the Si content.

and reversibility of CNTs) can be realized if Si particles are dispersed throughout CNTs by high-energy ball-milling.

In this study, SWCNTs have been used to produce the CNT/Si composites with Si powder by high-energy ball-milling. The research objective of the present work is to develop the SWCNT/Si composites as an anode for high-energy-density Li-ion rechargeable batteries and to analyze the charge/discharge characteristics for insertion/extraction of the Li ions into/from the SWCNT/Si composites.

2. EXPERIMENTAL SECTION

SWCNTs used in this work were synthesized on the supported catalysts by thermal chemical vapor deposition with a bundle type and then effectively purified by an acidic treatment followed by the gas-phase oxidation process.[26] Figure 1 shows the transmission electron microscopy (TEM) image of the purified SWCNTs with over 10 μm in length and about 30−50 nm in bundle diameter.

The SWCNT/Si composites were prepared by ball-milling of the purified SWCNTs and Si powder with a maximum particle size of 45 μm. In our previous study about the charge/discharge performance of the SWCNT/Si composites after ball-milling for 30 min as a function of the Si content, the SWCNT/Si composites with a 5:5 weight ratio of SWCNTs and Si appeared to have the highest reversible capacity and

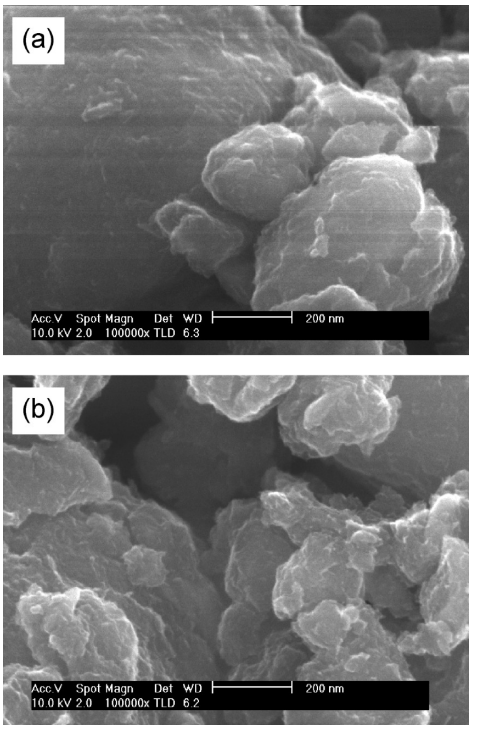

Figure 3. SEM images of the SWCNT/Si composites after ball-milling for (a) 30 and (b) 60 min.

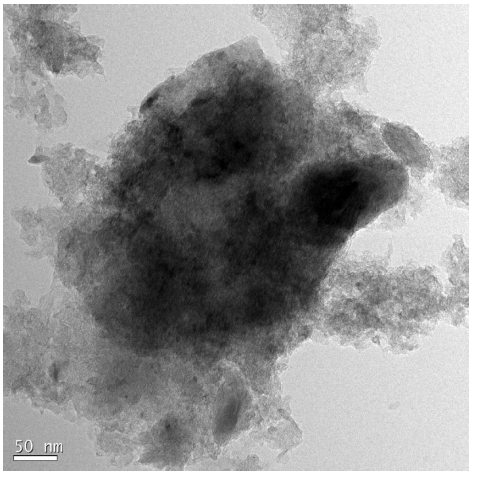

Figure 4. TEM image of the SWCNT/Si composites after ball-milling for 60 min.

lowest irreversible capacity, as shown in Figure 2. Thus, 50 mg mixtures of the purified SWCNTs of 50 wt % and Si powder of 50 wt % were ball-milled for 30 and 60 min in a stainless steel vial by an impact mode of a stainless steel ball. All of the samples were dried for 5 h at 150 °C in a 5 × 10^{-6} Torr vacuum before use.

The cell for the charge/discharge and cyclic voltammetry test consisted of Li foil and a SWCNT/Si film as the electrodes. The SWCNT/Si electrodes were prepared by coating slurries consisting of SWCNT/Si (85 wt %) with acetylene carbon black (5 wt %) and poly(vinylidene fluoride) (10 wt %) as a binder dissolved in a 1-methyl-2-pyrrolidinone solution on a stainless steel substrate. All of the SWCNT/Si electrodes were dried for 5 h at 150 °C in a 5 × 10^{-6} Torr vacuum. After drying, the weight of each sample was measured as about 2−4 mg. The

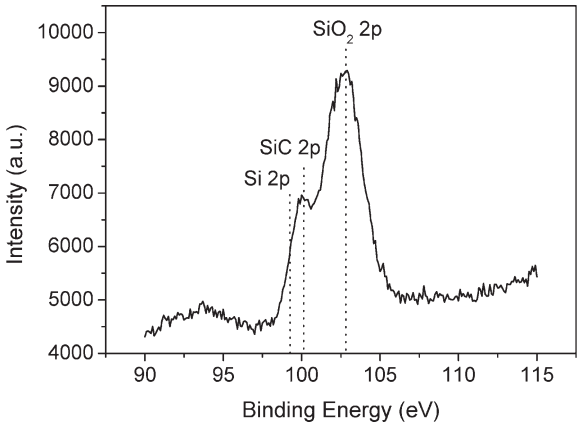

Figure 5. Si peaks in the XPS spectrum of the SWCNT/Si composites after ball-milling for 60 min. XPS analysis was measured at 15 kV and 20 mA using Al Kα.

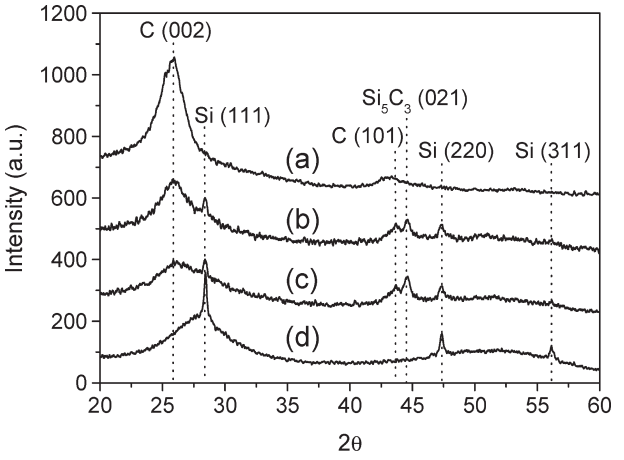

Figure 6. XRD patterns of (a) the purified SWCNTs and the SWCNT/Si composites after ball-milling for (b) 30 and (c) 60 min and of (d) Si powder.

Li/(SWCNT/Si) cells were assembled using a coin-type cell in an Ar-filled glovebox. A polypropylene filter soaked with liquid electrolyte, which was 1 M $LiPF_6$ dissolved in a 1:1 volume ratio of ethylene carbonate and dimethyl carbonate, was placed between the anode and cathode in the cell.

The charge/discharge test of the Li/(SWCNT/Si) cells was performed under galvanostatic mode. The cells were charged (insertion) and discharged (extraction) at a constant current of 50 mA g^{-1} (based on the weight of SWCNT/Si composites) between 0 and 3 V. The cyclic voltammetry test of the Li/(SWCNT/Si) cells was performed at a constant scan rate of 0.1 mV s^{-1} between 0 and 3 V.

3. RESULTS AND DISCUSSION

3.1. Structures of SWCNT/Si Composites. Figure 3 shows the scanning electron microscopy (SEM) images of the SWCNT/Si composites after ball-milling for 30 and 60 min. The SEM images indicate that the purified SWCNTs shown in Figure 1 were fractured, flattened, and densely packed around Si particles by ball-milling. The size of the Si particles in the SWCNT/Si composites was found to decrease slightly with the ball-milling time.

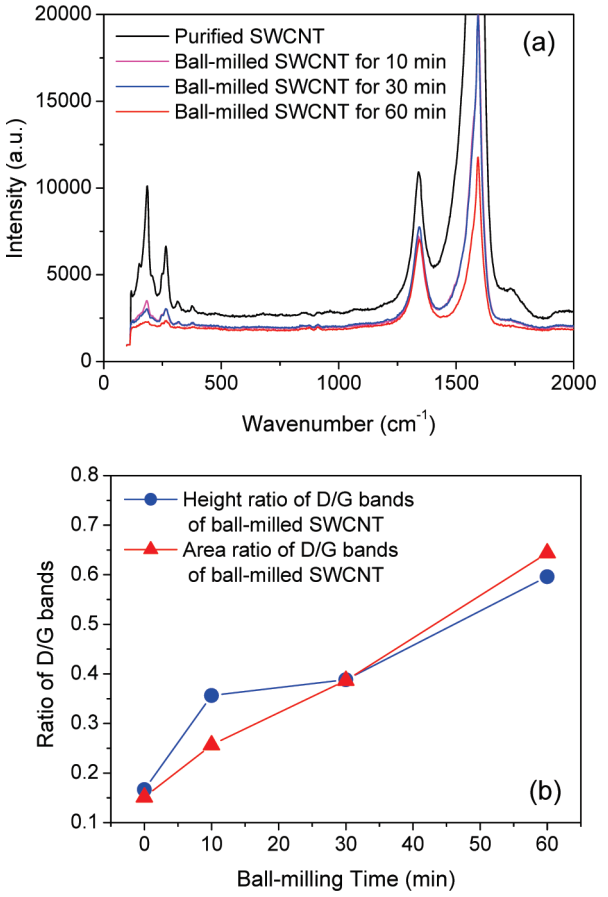

Figure 7. (a) Raman spectra of the purified SWCNTs and the ball-milled SWCNTs for 10, 30, and 60 min[12] and (b) the relative height and area ratios of the disordered C peak (D band) over the ordered C peak (G band) from Raman spectra of the ball-milled SWCNTs. The data were collected using an Ar-ion laser of 514.5 nm and a micro-Raman spectrometer with a CCD detector at room temperature.

Figure 4 shows the TEM image of the SWCNT/Si composites after ball-milling for 60 min, demonstrating clearly that the fractured and flattened SWCNTs were densely packed around Si particles by ball-milling. To examine the interface of the SWCNT/Si composites, X-ray photoelectron spectroscopy (XPS) analysis was applied to the SWCNT/Si composites. Figure 5 shows the Si peaks in the XPS spectrum of the SWCNT/Si composites after ball-milling for 60 min. In the SWCNT/Si composites, the peaks of three Si phases were observed: SiO_2 2p (~103 eV), SiC 2p (~100 eV), and Si 2p (~99 eV).[27] It is believed that the surface of the Si particles was oxidized by ball-milling, and the chemical-bonded SiC compound was formed on the interface of the SWCNTs and Si particles. This was also confirmed by X-ray diffraction (XRD) patterns of the SWCNT/Si composites after ball-milling for 30 and 60 min, as shown in Figure 6, indicating that the SiC compound (Si_5C_3) peaks were observed in the SWCNT/Si composites, with the peak intensity of the SiC compound increasing with the ball-milling time. Further, as the ball-milling time increased, the intensity of the (002) diffraction peak of the SWCNTs decreased and broadened.

Although the structures of the SWCNTs were destroyed practically after ball-milling, as shown in Figures 3 and 4, according to our previous work about the ball-milled SWCNTs,[12]

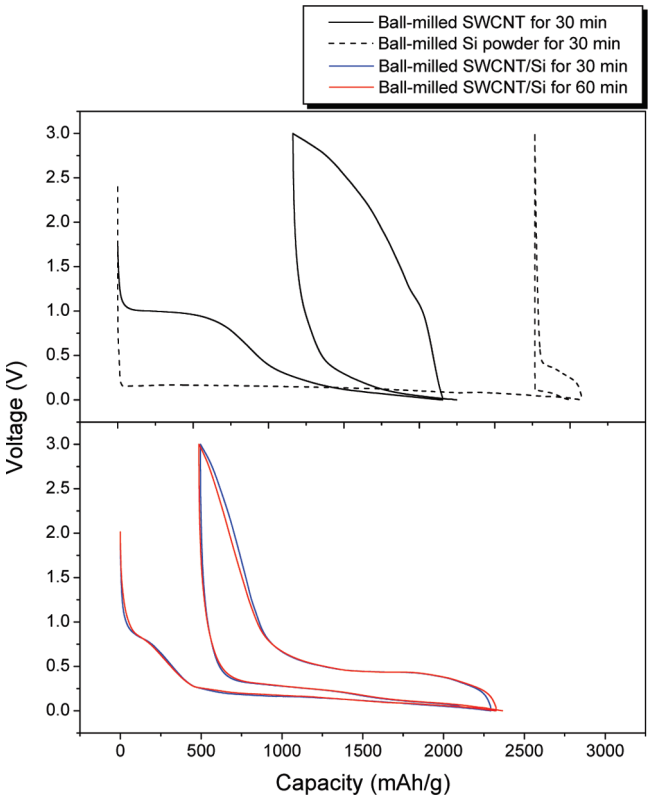

Figure 8. Charge/discharge characteristics for insertion/extraction of the Li ions into/from the ball-milled SWCNTs and Si powder for 30 min and the SWCNT/Si composites after ball-milling for 30 and 60 min.

Table 1. BET Specific Surface Area and Pore Volume of the Purified SWCNTs and the Ball-Milled SWCNTs for 30 min,[12] the SWCNT/Si Composites after Ball-Milling for 30 and 60 min, and Si Powder

	BET specific surface area ($m^2\ g^{-1}$)	total pore volume ($cm^3\ g^{-1}$)
Si powder	2.13	0.007
purified SWCNT	1059.12	1.01
ball-milled SWCNT for 30 min	810.94	0.44
ball-milled SWCNT/Si for 30 min	308.27	0.22
ball-milled SWCNT/Si for 60 min	285.21	0.15

it is believed that the SWCNTs in the SWCNT/Si composites maintained their structures after ball-milling. Raman spectra of the purified SWCNTs and the ball-milled SWCNTs for 10, 30, and 60 min are shown in Figure 7a.[12] Raman-active vibrational modes associated with the SWCNTs [the tangential modes (A_{1g}, E_{1g}, and E_{2g}) with peak positions around 1600 cm^{-1}; G band, the radial breathing mode with peak position around 186 cm^{-1}] and disordered C (the broad peaks around 1350 cm^{-1}; D band) were observed in all samples. However, the relative height and area ratios of the disordered C peak (D band) over the ordered C peak (G band) increased substantially with the ball-milling time (Figure 7b). This indicates that ball-milling resulted in a significant increase in the intensity of the disordered C mode with broadening of the SWCNT peaks, suggesting that SWCNTs were converted to the disordered/amorphous C by ball-milling.

3.2. Charge/Discharge Characteristics of the SWCNT/Si Composites. Figure 8 shows the charge/discharge characteristics for insertion/extraction of the Li ions into/from the SWCNT/Si composites after ball-milling for 30 and 60 min. The reversible capacity (C_{rev}) is defined as the first discharge capacity, while the irreversible capacity (C_{irr}) is defined as the difference between the first charge and discharge capacities. For the ball-milled Si powder, C_{rev} was very low, although the Li-insertion capacity was very high, above 3000 mAh g^{-1}. C_{rev} of the SWCNT/Si composites after ball-milling for 30 min increased from 988 mAh g^{-1} for the ball-milled SWCNTs for 30 min to 1799 mAh g^{-1}, and C_{irr} decreased from 1170 to 496 mAh g^{-1}. In addition, C_{rev} of the SWCNT/Si composites after ball-milling for 60 min increased slightly to 1845 mAh g^{-1}, and C_{irr} decreased slightly to 474 mAh g^{-1}. Therefore, the Coulombic efficiency of the SWCNT/Si composites increased from 46% in the ball-milled SWCNTs for 30 min to 80% after ball-milling for 60 min. The charge/discharge characteristics for several samples, taken from different batches measured under the same conditions, showed small deviation values of the capacities in the range of $\pm$30 mAh g^{-1}.

The charge/discharge curves of the SWCNT/Si composites exhibited a different curve shape with the ball-milled SWCNTs and Si powder, indicating that the mechanism of insertion/extraction of the Li ions into/from the SWCNT/Si composites was different from that of the ball-milled SWCNTs and Si powder, as shown in Figure 8. In the SWCNT/Si composites, the small voltage hysteresis with a large voltage plateau was observed in the charge/discharge curves.

The voltage plateau at 0.8 V appearing in the first charge curves shown in Figure 8 has been attributed to decomposition of the electrolyte and formation of SEI on the surface of SWCNTs, which result in C_{irr} in the SWCNT/Si composites.[11,12] The voltage plateau at 0.8 V is proportional to the surface area of SWCNTs on which the SEI is formed. The Brunauer–Emmett–Teller (BET) specific surface area and the pore volume of the SWCNT/Si composites after ball-milling for 30 and 60 min are compared with that of the purified SWCNTs and the ball-milled SWCNTs for 30 min and Si powder, as shown in Table 1. The specific surface area and the pore volume of the SWCNT/Si composites were smaller than that of the ball-milled SWCNTs and decreased with the ball-milling time. The decrease in the specific surface area and the pore volume of the SWCNT/Si composites indicates that the SWCNT/Si composites have densely packed structures due to fracture and flattening of the purified SWCNTs around Si particles by ball-milling. The increase in the packing density of the SWCNT/Si composites is believed to be the reason for the reduction in C_{irr} and the voltage plateau at 0.8 V in the SWCNT/Si composites. Following the voltage plateau at 0.8 V, the voltage declined with a sloping profile, and most of the Li ions were inserted into SWCNTs and alloyed with Si particles in the SWCNT/Si composites below 0.2 V. It is believed that most of the inserted Li ions were alloyed with Si particles, and then the LiSi compound was formed during the first charge process.

In the charge/discharge curves in Figure 8, most of the Li ions were extracted at 0.5 V with the voltage plateau from the SWCNT/Si composites. It appears that most of the extracted

Li ions from the SWCNT/Si composites were dealloyed with Si particles because the inserted Li ions into SWCNTs were extracted uniformly between 0 and 3 V with a large voltage hysteresis.[12] However, in the ball-milled Si powder, the Li ions extracted by dealloying with Si particles were small because Si particles were crumbled because of the large volume expansion and brittleness of the LiSi compound formed during Li insertion and, hence, insulated from the current collector.[15]

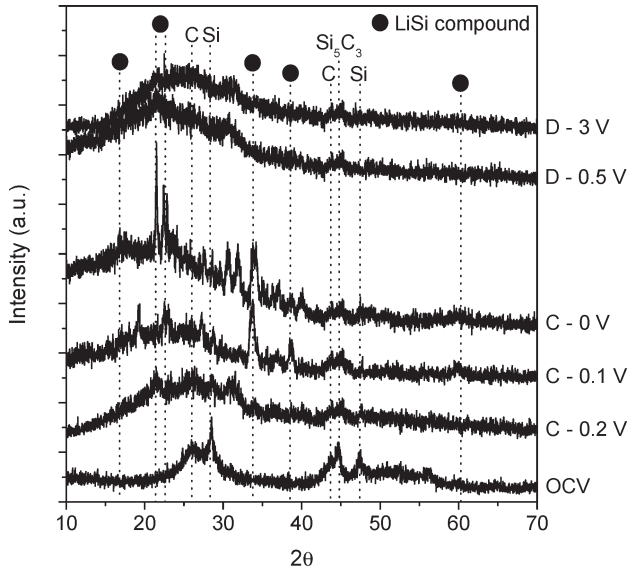

Figure 9. XRD patterns at different voltage stages during the first charge/discharge process of the SWCNT/Si composites after ball-milling for 60 min.

To examine the insertion/extraction of the Li ions into/from the SWCNT/Si composites after ball-milling for 60 min, XRD experiments were performed at different voltage stages during the first charge/discharge process, and the results are shown in Figure 9. The SWCNTs, Si, and SiC compound diffraction peaks at the open-circuit voltage (OCV) for the SWCNT/Si composites were observed in the first charge process. The LiSi compound peaks appeared below 0.2 V during the first charge process, and the intensities of the LiSi compound peaks charged to 0.1 and 0 V increased significantly. It is evident from the increase in the diffraction peaks of the LiSi compound for the SWCNT/Si composites charged to 0 V that most of the Li ions appear to be alloyed with Si particles in the SWCNT/Si composites. In the first discharge process, the LiSi compound peaks were not observed above 0.5 V, indicating that the Li ions alloyed with Si particles were dealloyed below 0.5 V in the first discharge process. Interestingly, the crystalline structure of Si particles appears to be converted to an amorphous structure during dealloying with Li ions in the first discharge process, which was confirmed by the disappearance and broadening of Si diffraction peaks at 3 V.

The SWCNTs around Si particles in the SWCNT/Si composites may contribute to the prevention of electrical isolation of Si particles by the crumbling of Si particles in the charge/discharge

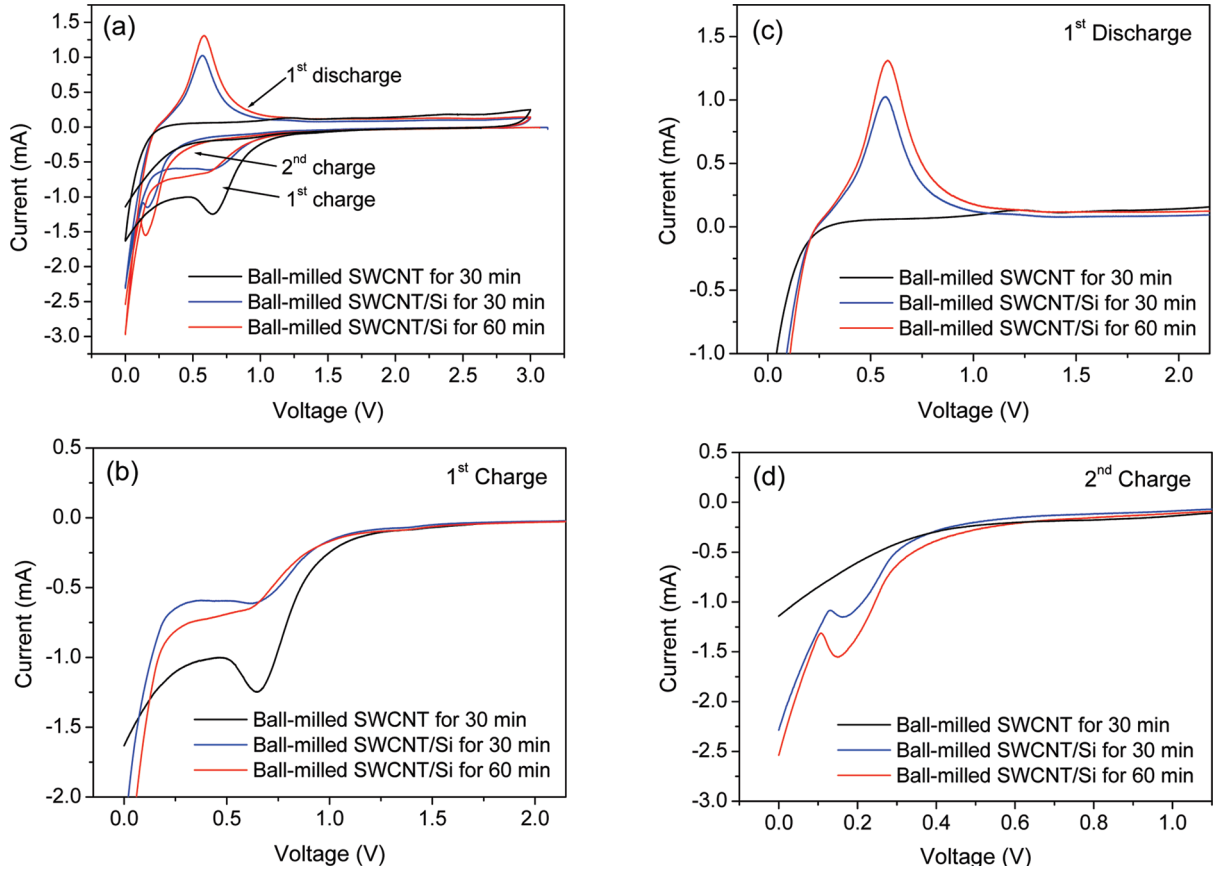

Figure 10. (a) Cyclic voltammetry curves of the ball-milled SWCNTs for 30 min and the SWCNT/Si composites after ball-milling for 30 and 60 min, (b) the first charge, (c) the first discharge, and (d) the second charge cyclic voltammetry curves.

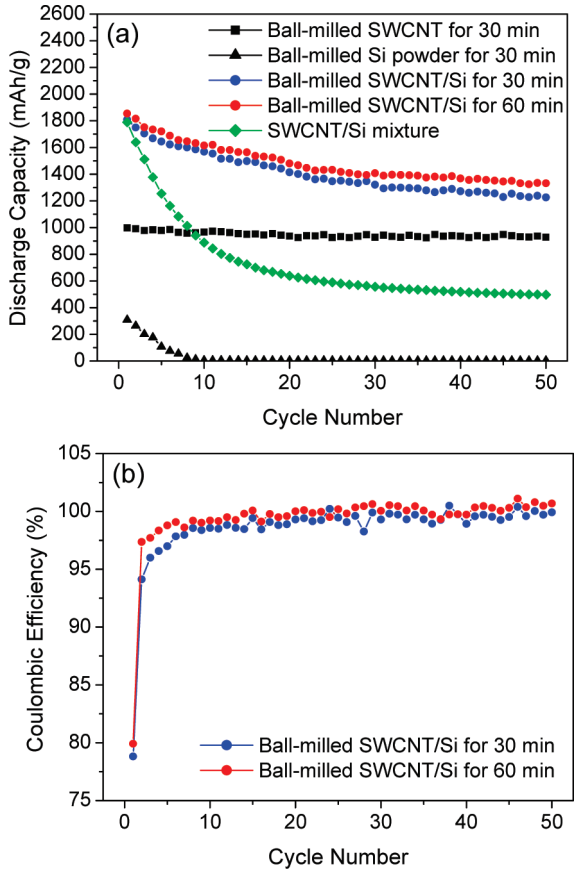

Figure 11. (a) Discharge capacities and (b) Coulombic efficiencies of the SWCNT/Si composites after ball-milling for 30 and 60 min as a function of the cycle number.

process because of their high electron conductivity. Therefore, the SWCNTs covered well around Si particles are very important to the enhancement of C_{rev} in the SWCNT/Si composites. Most of the Li ions were inserted into the SWCNT/Si composites by alloying with Si particles and extracted from the SWCNT/Si composites by dealloying with Si particles well covered by SWCNTs. The ball-milling contributed to the decrease in the particle size of SWCNTs and Si particles and SWCNTs to the well covering around Si particles in the SWCNT/Si composites.

3.3. Cyclic Voltammetry Behaviors of the SWCNT/Si Composites. Figure 10 shows the cyclic voltammetry curves of the SWCNT/Si composites after ball-milling for 30 and 60 min. The cyclic voltammetry curves of all samples clearly show the peaks corresponding to insertion and extraction of the Li ions. The peak around 0.8 V appearing in the first charge cyclic voltammetry curves shown in Figure 10b, corresponding to the voltage plateau at 0.8 V in the first charge curve shown in Figure 8, is due presumably to an irreversible reaction for the SEI formation during Li insertion into the SWCNT/Si composites.[12] The integrated peak area around 0.8 V for the SWCNT/Si composites decreased, indicating that the specific surface area for the SEI formation decreased in the SWCNT/Si composites due to an increase in the packing density of the SWCNT/Si composites.

In the first discharge cyclic voltammetry curves shown in Figure 10c, the peaks around 0.2 and 0.5 V for the SWCNT/Si composites were observed, but the intensity of the 0.2 V peak was much lower than that of the 0.5 V peak. The peaks around 0.2 and 0.5 V are attributed to extraction of the Li ions from SWCNTs[12] and to dealloying of the Li ions from Si particles, respectively, but the extracted Li ions from SWCNTs are much smaller than the Li ions dealloyed with Si particles. In the second charge cyclic voltammetry curves shown in Figure 10d, the peak around 0.2 V for the SWCNT/Si composites was observed. The peak around 0.2 V is attributed to insertion of the Li ions into SWCNTs[12] and to alloying of the Li ions with Si particles, but the Li ions alloyed with Si particles are much larger than those of the Li ions inserted into SWCNTs. As the ball-milling time increased, the intensity of peaks around 0.5 V in Figure 10c and 0.2 V in Figure 10d increased, indicating that the Li ions dealloyed and alloyed with Si particles increased in the SWCNT/Si composites. It appears that the ball-milling contributed to a decrease in the particle size of SWCNTs and Si particles, and SWCNTs to cover well around Si particles in the SWCNT/Si composites. Therefore, the Li ions alloyed and dealloyed with Si particles increased in the SWCNT/Si composites with the ball-milling time.

3.4. Cycle Life Behaviors of the SWCNT/Si Composites. Figure 11 shows the discharge capacity and Coulombic efficiency of the SWCNT/Si composites after ball-milling for 30 and 60 min as a function of the cycle number. In the cycle curves shown in Figure 11a, the ball-milled Si powder presented a limited capacity related to the crumbling of the LiSi compound due to large volume expansion during Li insertion and brittleness of the LiSi compound. However, the ball-milled SWCNTs presented almost stable capacities, which slightly decreased and maintained 94% (928 mAh g^{-1}) of their initial capacity (988 mAh g^{-1}) after 50 cycles. It is evident from Figure 11a that the discharge capacities of the SWCNT/Si composites increased slightly with the ball-milling time; the SWCNT/Si composites after ball-milling for 30 min maintained 68% (1226 mAh g^{-1}) of their initial capacity (1799 mAh g^{-1}), and the SWCNT/Si composites after ball-milling for 60 min maintained 72% (1332 mAh g^{-1}) of their initial capacity (1845 mAh g^{-1}) after 50 cycles. The Coulombic efficiencies for the SWCNT/Si composites also increased slightly with the ball-milling time, as shown in Figure 11b.

To investigate the effect of ball-milling on the cycle performance of the SWCNT/Si composites, the discharge capacity of the SWCNT/Si mixture of 50/50 wt.% as a function of the cycle number is shown in Figure 11 (a). The first discharge capacity (1716 mAh g-1) of the SWCNT/Si mixture was slightly lower than that of the SWCNT/Si composites after ball-milling for 30 and 60 min. The discharge capacity of the SWCNT/Si mixture decreased abruptly up to 10 cycles which was similar to the cycle behavior of Si powder, and then slightly decreased and maintained 29% (496 mAh g-1) of their initial capacity after 50 cycles.

It appears that the cycle performance of the SWCNT/Si composites was improved by high energy ball-milling. By high energy ball-milling, the particle size of SWCNTs and Si particles decreased, and SWCNTs of high electron conductivity covered well around Si particles in the SWCNT/Si composites. The SWCNTs around Si particles contributed to prevent Si particles from electrical isolating by the crumbling of Si particles during the cycling process. In addition, the chemical bonded SiC compound formed on the interface of SWCNTs and Si particles by high energy ball-milling enhanced the interparticle contact during the cycling process. These factors appeared to enhance the cycle performance of the SWCNT/Si composites with the increase in the ball-milling time.

4. CONCLUSIONS

The SWCNT/Si composites produced by high-energy ball-milling exhibited a structure in which Si particles were densely packed by the flattened and fractured SWCNTs. In addition, the SiC compound formed on the SWCNT/Si interface made a strong contact between SWCNTs and Si particles.

The highest C_{rev} and lowest C_{irr} of the SWCNT/Si composites were measured to be 1845 and 474 mAh g^{-1} after ball-milling for 60 min, respectively. Therefore, the Coulombic efficiency of the SWCNT/Si composites increased from 46% in the ball-milled SWCNTs for 30 min to 80% after ball-milling for 60 min. The charge/discharge curves of the SWCNT/Si composites exhibited a different curve shape with SWCNTs and Si powder, demonstrating a small voltage hysteresis with the large voltage plateau observed in the charge/discharge curves. During the charge/discharge process, most of the Li ions were inserted into the SWCNT/Si composites by alloying with Si particles below 0.2 V and were extracted from the SWCNT/Si composites by dealloying with Si particles around 0.5 V.

During the cycling process, the discharge capacity and Coulombic efficiency of the SWCNT/Si composites increased slightly with the ball-milling time. These results were due primarily to the fact that SWCNTs provided a flexible conductive matrix that compensated for the dimensional changes of Si particles during Li insertion and avoided loosening of the interparticle contacts during the crumbling of Si particles. The ball-milling contributed to a decrease in the particle size of SWCNTs and Si particles and to an increase in the electrical contact between SWCNTs and Si particles in the SWCNT/Si composites. These factors enhanced the Li storage capacity and cycle performance of the SWCNT/Si composites during the charge/discharge process.

AUTHOR INFORMATION

Corresponding Author

*Telephone: +82-42-350-3326. Fax: +82-42-350-3310. E-mail: hskwon@kaist.ac.kr.

Present Addresses

†Battery Development Team, Energy Business Division, Samsung SDI Co., Ltd., 508, Sungsung-dong, Cheonan, Chungcheongnam-do, 330-300, Korea. Telephone: +82-70-7125-0387. Fax: +82-41-560-3696. E-mail: jyeom74@gmail.com.

ACKNOWLEDGMENT

This work was supported by the Growth Engine Technology Development Program (Project No. 10016472) and the BK21 program funded by Korea Ministry of Knowledge Economy.

REFERENCES

(1) Maurin, G.; Bousquet, C.; Henn, F.; Bernier, P.; Almairac, R.; Simon, B. *Chem. Phys. Lett.* **1999**, *312* (1), 14–18.
(2) Wu, G. T.; Wang, C. S.; Zhang, X. B.; Yang, H. S.; Qi, Z. F.; He, P. M.; Li, W. Z. *J. Electrochem. Soc.* **1999**, *146* (5), 1696–1701.
(3) Ishihara, T.; Kawahara, A.; Nishiguchi, H.; Yoshio, M.; Takita, Y. *J. Power Sources* **2001**, *97−98*, 129–132.
(4) Frackowiak, E.; Gautier, S.; Gaucher, H.; Bonnamy, S.; Beguin, F. *Carbon* **1999**, *37*, 61–69.
(5) Yang, Z. H.; Wu, H. Q. *Solid State Ionics* **2001**, *143*, 173–180.
(6) Kumar, T. P.; Stephan, A. M.; Thayananth, P.; Subramanian, V.; Gopukumar, S.; Renganathan, N. G.; Raghavan, M.; Muniyandi, N. *J. Power Sources* **2001**, *97−98*, 118–121.
(7) Eom, J. Y.; Kwon, H. S.; Liu, J.; Zhou, O. *Carbon* **2004**, *42* (12−13), 2589–2596.
(8) Eom, J. Y.; Kim, D. Y.; Kwon, H. S. *J. Power Sources* **2006**, *157* (1), 507–514.
(9) Gao, B.; Kleinhammes, A.; Tang, X. P.; Bower, C.; Fleming, L.; Wu, Y.; Zhou, O. *Chem. Phys. Lett.* **1999**, *307* (7), 153–157.
(10) Claye, A. S.; Fischer, J. E.; Huffman, C. B.; Rinzler, A. G.; Smalley, R. E. *J. Electrochem. Soc.* **2000**, *147* (8), 2845–2852.
(11) Gao, B.; Bower, C.; Lorentzen, J. D.; Fleming, L.; Kleinhammes, A.; Tang, X. P.; McNeil, L. E.; Wu, Y.; Zhou, O. *Chem. Phys. Lett.* **2000**, *327* (9), 69–75.
(12) Eom, J. Y.; Kwon, H. S. *J. Mater. Res.* **2008**, *23* (9), 2458–2466.
(13) Shimoda, H.; Gao, B.; Tang, X. P.; Kleinhammes, A.; Fleming, L.; Wu, Y.; Zhou, O. *Physica B* **2002**, *323*, 133–134.
(14) Shimoda, H.; Gao, B.; Tang, X. P.; Kleinhammes, A.; Fleming, L.; Wu, Y.; Zhou, O. *Phys. Rev. Lett.* **2002**, *88* (1), 015502-1-4.
(15) Wang, C. S.; Wu, G. T.; Zhang, X. B.; Qi, Z. F.; Li, W. Z. *J. Electrochem. Soc.* **1998**, *145* (8), 2751–2758.
(16) Gao, B.; Sinha, S.; Fleming, L.; Zhou, O. *Adv. Mater.* **2001**, *13* (11), 816–819.
(17) Boukamp, B. A.; Lesh, G. C.; Huggins, R. A. *J. Electrochem. Soc.* **1981**, *128* (4), 725–729.
(18) Yang, J.; Winter, M.; Besenhard, J. O. *Solid State Ionics* **1996**, *90* (1−4), 281–287.
(19) Wang, G. X.; Ahn, J. H.; Yao, J.; Bewlay, S.; Liu, H. K. *Electrochem. Commun.* **2004**, *6* (7), 689–692.
(20) Holzapfel, M.; Buqa, H.; Scheifele, W.; Novak, P.; Petrat, F. M. *Chem. Commun.* **2005**, *12*, 1566–1568.
(21) Kim, T.; Mo, Y. H.; Nahm, K. S.; Oh, S. M. *J. Power Sources* **2006**, *162*, 1275–1281.
(22) Shu, J.; Li, H.; Yang, R.; Shi, Y.; Huang, X. *Electrochem. Commun.* **2006**, *8*, 51–54.
(23) Park, S.; Kim, T.; Oh, S. M. *Electrochem. Solid-State Lett.* **2007**, *10*, A142–A145.
(24) Zhang, Y.; Zhang, X. G.; Zhang, H. L.; Zhao, Z. G.; Li, F.; Liu, C.; Cheng, H. M. *Electrochim. Acta* **2006**, *51*, 4994–5000.
(25) Lestriez, B.; Desaever, S.; Danet, J.; Moreau, P.; Plée, D.; Guyomard, D. *Electrochem. Solid-State Lett.* **2009**, *12*, A76–A80.
(26) Zheng, B.; Li, Y.; Liu, J. *Appl. Phys. A: Mater. Sci. Process.* **2002**, *74*, 345–248.
(27) Yang, Z. H.; Jia, D. C.; Duan, X. M.; Zhou, Y. *J. Non-Cryst. Solids* **2010**, *356*, 326–333.